Carbon 229 (2024) 119534

Contents lists available at ScienceDirect

Carbon

journal homepage: www.elsevier.com/locate/carbon

Highly reliable and ultra-wideband metamaterial absorber based on graphene-assembled films for extremes

Yu Zhou [a,c], Bilei Zhou [b], Shiyi Jin [a], Zhi Luo [a], Wei Qian [a,c], Jiannan Guo [a], Baowen Li [c], Haoran Zu [a,d], Rongguo Song [a,b,**], Daping He [a,*]

[a] Hubei Engineering Research Center of RF-Microwave Technology and Application, School of Science, Wuhan University of Technology, Wuhan, 430070, China
[b] Air Force Early Warning Academy, Wuhan, 430019, China
[c] State Key Laboratory of Advanced Technology for Materials Synthesis and Processing, Wuhan University of Technology, Wuhan, 430070, China
[d] School of Information Engineering, Wuhan University of Technology, Wuhan, 430070, China

ARTICLE INFO

Keywords:
Graphene-assembled film
Metamaterial absorber
Highly reliable
Ultra-wideband
Extremes

ABSTRACT

Metamaterial absorbers have demonstrated significant potential in mitigating electromagnetic pollution, yet there is a dearth of research on absorbers that function effectively in extreme environments. In this work, a highly reliable and ultra-wideband metamaterial absorber based on graphene-assembled films (GAFs) is proposed. The presented absorber consists of four-layer structures, including a high-resistance GAF pattern layer, a polyimide medium layer, an air layer, and a low-resistance GAF layer. The periodic ring structure made of high-resistance GAF by screen printing with a sheet resistance of 57 Ω/sq exhibits excellent characteristics of wide-band absorption and broad incidence angle absorption. The GAF absorber demonstrates a measured absorption efficiency exceeding 90 %, covering 4.24–17.90 GHz, and has a relative bandwidth of 123.4 %, which exhibits good stability when electromagnetic waves are incident at 0–30°. More importantly, the GAF absorber maintains excellent performance in various extreme conditions, including acid, alkali, salt spray, high-humidity, high-temperature, and low-temperature environments. Therefore, the GAF absorber demonstrates consistent reliability and stability under extreme conditions, which is significant for electromagnetic protection under extremes.

1. Introduction

Electromagnetic metamaterials, as an artificially designed sub-wavelength structure capable of tailoring the electromagnetic response, have a wide range of applications in electromagnetic stealth and protection [1–3]. By meticulously designing the shape, size, material, and arrangement, metamaterial absorbers (MMAs) can effectively absorb electromagnetic energy on their surfaces and convert it primarily into heat, minimizing reflection [4–6]. However, the narrow band characteristics caused by resonant mechanisms have limited their practical application in both civil and military fields [7–9]. Additionally, there is an increasing demand for wideband metamaterial absorbers that work reliably under extreme environmental conditions [10–12]. Consequently, the development of wideband MMAs that can meet these demands remains a significant scientific and technological challenge.

Many methods have been proposed in recent years to expand the working bandwidth of MMA, such as combining multiple resonant points, introducing concentrated elements, and adopting resistance films [13–15]. To combine multiple resonance points, researchers have expanded the working bandwidth of the absorber by arranging subunits working at different frequencies in plane [16–19] and space [20–23]. Nevertheless, these methods increase the design complexity, the number of conductor layers, as well as the profile and weight of the absorber. Another common method is to load lumped elements such as resistors, inductors, capacitors, and diodes, especially resistors, to reduce the quality factor and increase the bandwidth of the absorption peak. Some metamaterial absorbers loaded with lumped elements [24–27] also have tunable features [28]. However, integrating equivalent lumps brings challenges in maintaining miniaturization and a low profile. In addition, there are three-dimensional structures that can be used to achieve

* Corresponding author.
** Corresponding author. Hubei Engineering Research Center of RF-Microwave Technology and Application, School of Science, Wuhan University of Technology, Wuhan, 430070, China.
E-mail addresses: rongguo_song@whut.edu.cn (R. Song), hedaping@whut.edu.cn (D. He).

https://doi.org/10.1016/j.carbon.2024.119534
Received 21 April 2024; Received in revised form 26 July 2024; Accepted 7 August 2024
Available online 8 August 2024

broadband wave absorption [29,30]. Moreover, most absorbers are composed of metals, which not only present challenges in realizing ultra-broadband absorption but are also not resistant to extreme environments such as acids, alkalis, salts, high humidity, and high and low temperatures.

In this work, we propose a low-profile metamaterial absorber based on graphene-assembled films (GAFs) with varying resistance to achieve ultra-wideband working bandwidth and the ability to cope with extreme environments. The high-resistance graphene-assembled film (HGAF) pattern layer with a resistance of 57 Ω/sq is prepared using graphene ink through the screen printing process. The graphene-assembled film with a low resistance (LGAF) of 0.03 Ω/sq is utilized as the reflection layer. Experimental results of the fabricated low-profile and ultra-wideband MMA demonstrate good agreement with simulation results. It is worth noting that the MMA displayed absorptance of over 90 % in the frequency range of 4.24–17.90 GHz, with a relative bandwidth of 123.4 %. Moreover, the MMA can retain its structural integrity and dependable performance even in extreme conditions, exhibiting a relative bandwidth of approximately 110 %.

2. Characterization of graphene-assembled films

Graphene, renowned for its two-dimensional structure, has proven to be an incredibly versatile material, particularly in applications aimed at electromagnetic protection [31]. In our research, the use of two distinct types of impedance graphene-assembled films (GAFs) to design metamaterial absorbers is a strategic approach to enhancing their effectiveness. The HGAF pattern layer made of graphene ink with a resistance of 57 Ω/sq is purchased from Wuhan Hanene Technology Co., Ltd. by screen printing, which has broad application prospects and is more beneficial for mass manufacturing. In addition, the LGAF layer with a resistance of 0.03 Ω/sq is fabricated in our previous work [32–34].

Fig. 1(a) shows the physical appearance of the two kinds of GAFs, which are 10 × 10 cm and capable of large-scale production. As shown in X-ray diffraction (XRD) patterns in Fig. 1(b), both GAFs exhibit sharp and strong 002 diffraction peaks near 26.5°, and the corresponding interlayer spacing is 0.335 nm, which is similar to the interlayer spacing in graphite, indicating that the GAFs form a layered stacked structure and have a high degree of graphitization. As illustrated in Fig. 1(c), the D-peak of the LGAF is nearly zero at 1583 cm^{-1} in Raman spectra, indicating its high degree of graphitization and minimal defects. Conversely, the HGAF displays an obvious D-peak, indicating the presence of amorphous carbon and defects. It is apparent from Fig. 1(d) and (h) that both GAFs exhibit flexibility and can be easily bent. It can be seen from the scanning electron microscope that the LGAF has no cracks and holes (Fig. 1(e)), and the cross-section is dense, showing layers of stacking structure (Fig. 1(f)), which is conducive to electron transport. However, the surface of the HGAF has obvious holes (Fig. 1(i)), and the cross-section presents a disordered stacking structure (Fig. 1(j)), which is not conducive to the transmission of electrons, thereby reducing the conductivity of the film.

3. Results and discussion

3.1. The design of the metamaterial absorber

Fig. 2(a) depicts the schematic of the GAF MMA and the geometry of unit cell. The presented GAF absorber consists of four-layer structures, including a HGAF pattern layer, a polyimide medium layer, an air layer, and a LGAF layer. The HGAF pattern layer with polyimide ($\varepsilon_r = 3.5$, $\tan\delta = 0.0027$) is placed on the top of the air layer. The geometrical parameters shown in Fig. 2(a) were determined to be $p = 15$, $r = 4$, $w = 3.2$, $d = 5.8$, $t = 0.05$,and $c = 0.025$(mm). The design and simulation of the GAF MMA was performed using CST Microwave Studio. The unit cell structure is simulated with periodic boundary conditions along the x and y axes, while Floquet port excitations are applied along the z direction,

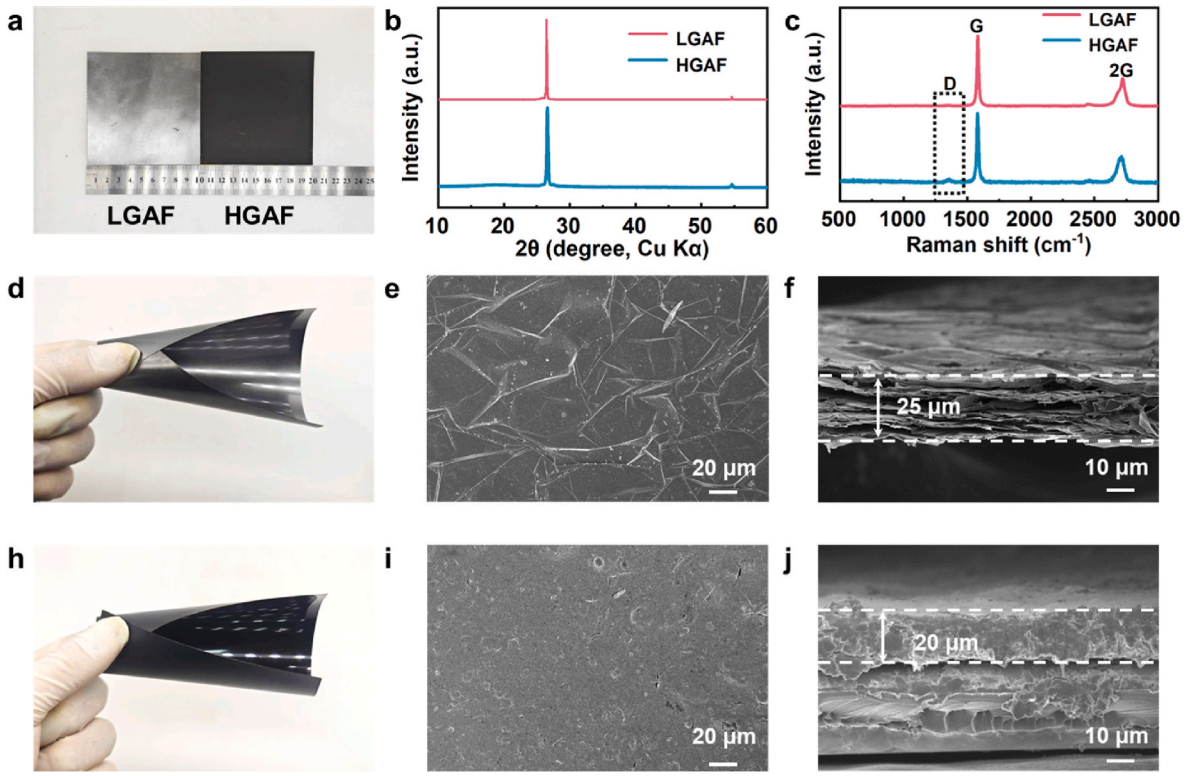

Fig. 1. Characterization of the GAFs. (a) The digital photo of the HGAF and LGAF. (b) and (c) X-ray diffraction patterns (b) and Raman spectra (c) of the two kinds of GAFs. (d) Flexible property of the LGAF. (e) Scanning electron microscope (SEM) image of the LGAF surface. (f) Cross-section SEM image of the LGAF. (h) Flexible property of the HGAF. (i) SEM image of the HGAF surface. (j) Cross-section SEM image of the HGAF.

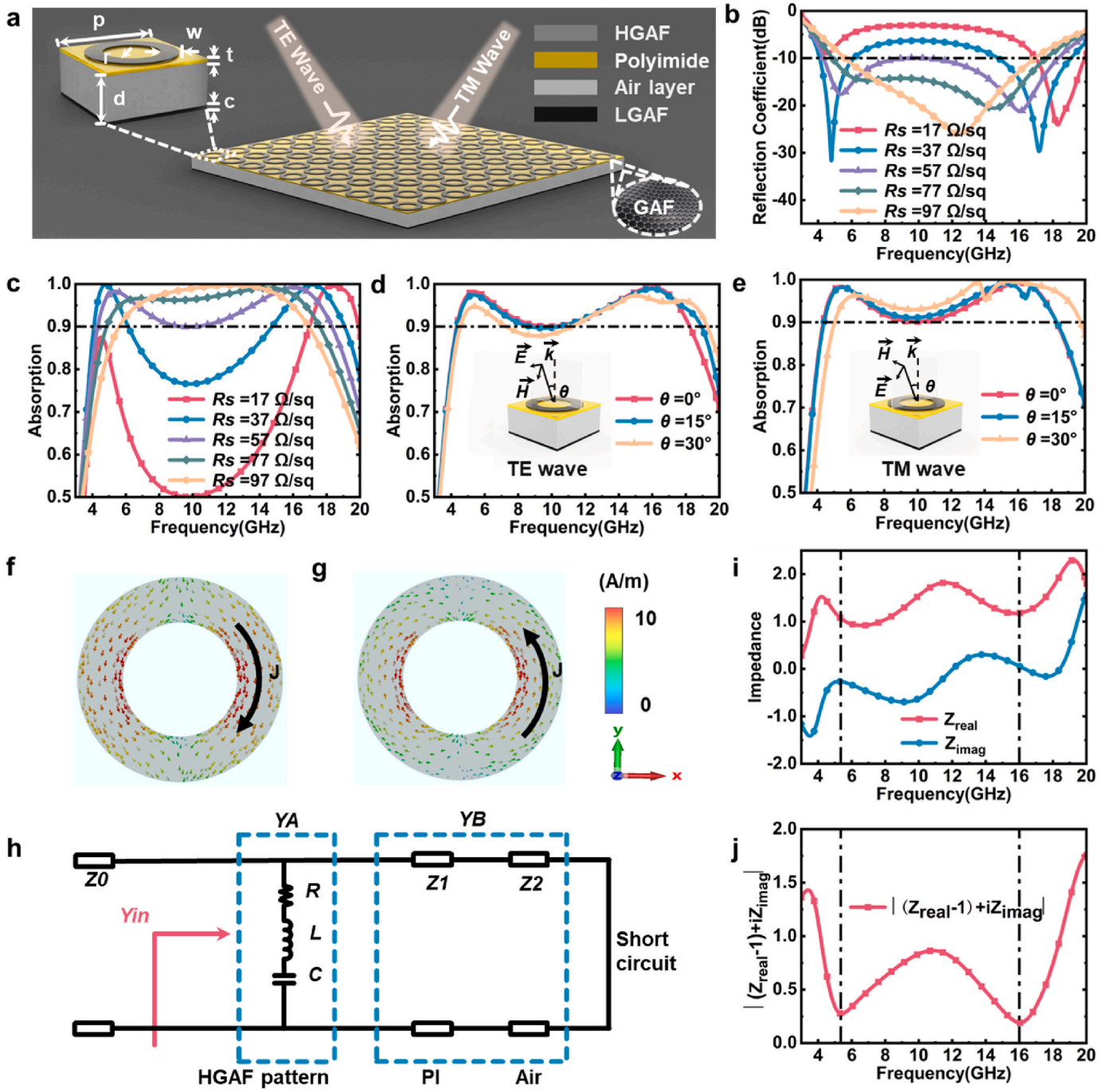

Fig. 2. (a). Schematic and unit cell geometry of the GAF MMA. (b) and (c) Simulated reflection coefficient (b) and absorption (c) of the GAF MMA for different values of the HGAF resistance(*Rs*). (d) and (e) Simulated absorption at incident angles of 0°, 15°, and 30° for the TE radiation (d) and TM radiation (e). (f) and (g) Surface current distribution of high-resistance graphene pattern layer at (f) 5.36 GHz and (g) 16.00 GHz. (h) Equivalent circuit of the GAF MMA. (i) and (j) The complex impedance (i) and the |(Zreal − 1) + iZimag)| (j) of the proposed GAF MMA.

both above and below the unit cell.

The absorption of the designed wideband MMA can be calculated by the formula

$$A(\omega) = 1 - R(\omega) - T(\omega) = 1 - |S_{11}|^2 - |S_{21}|^2 \quad (1)$$

where $R(\omega)$ is the reflection, and $T(\omega)$ is the transmission. The bottom surface is a LGAF layer with nearly total reflection [35], so the weak transmission can be ignored when calculating the absorption. To illustrate the effect of the HGAF pattern layer, the absorption responses of the proposed MMA are studied for different values of the HGAF resistance(*Rs*). It is observed from Fig. 2(b) and (c) that with the resistance of HGAF increasing, the two absorption peaks move towards each other, which increases the overall absorption level but simultaneously reduces the absorption bandwidth. In order to balance absorption efficiency and working bandwidth, the HGAF with resistance of 57 Ω/sq is selected for the surface ring pattern, thus resulting in the widest absorption bandwidth (above 90 %). According to the simulation results, the absorption rate of the GAF ultra-wideband MMA exceeds 90 % in the frequency range of 4.24–17.90 GHz, and the relative bandwidth reaches 123.4 %.

In addition, the proposed GAF MMA is compared with representative previous designs in terms of relative bandwidth and relative thickness. The relative bandwidth (reflection coefficient of −10 dB, or absorption

of 90 %) of the MMA is defined with respect to its center operation frequency, while the relative thickness is defined as the ratio of total thickness to the longest operation wavelength (λ). As shown in Table S1, the proposed GAF MMA achieves a remarkable relative bandwidth approaching 124.3 % within a total thickness of 0.084 λ. Notably, compared with references [36–42], the GAF MMA demonstrates both wider relative bandwidth and lower relative thickness simultaneously.

Fig. 2(d) and (e) show the simulated absorption of the proposed MMA for both transverse electric (TE) wave and transverse magnetic (TM) wave under normal incidence. For TE wave, with incident angle (θ) increases from 0° to 15°, the GAF MMA maintains an absorption of more than 90 % over the working frequency band. The boundary value at the high frequency of the absorption band is even widened to 18.93 GHz, which provides a relative bandwidth of 126.9 %. As the incident angle increased to 30°, the absorption of the proposed MMA slightly decreased between 7.36 GHz and 11.08 GHz, with a minimum absorption of 87.83 %. For TM wave, while θ increases from 0° to 15°, the GAF MMA also maintains an absorption rate of more than 90 %. As θ continues to increase to 30°, the working frequency range of the MMA moves to a higher frequency overall. The absorption of the MMA for TM polarized waves is greatly affected by the incident angle θ but remains above 90 % from 5.20 GHz to 19.75 GHz. As shown in Fig. S1, the absorption of TE wave is better than that of TM wave in the low-frequency band at oblique incidence. Under both TE and TM incidence conditions, absorption stays over 80 % for most frequencies and at oblique angles up to 50°. To analyze the mechanism of electromagnetic wave absorption, the surface current distribution of the HGAF pattern layer at two absorption peaks of 5.36 GHz and 16.00 GHz are shown in Fig. 2(f) and (g). Similarly, the electric field, magnetic field, and power loss density distribution at the two absorption frequency points of the HGAF pattern layer are shown in Fig. S2–4 respectively. At 5.36 GHz, the majority of surface current is concentrated on the inner side of the ring pattern, while a portion of current is uniformly distributed throughout the entire ring. Moreover, the concentration of current on the inner side of the ring pattern is higher at 16 GHz compared to 5.36 GHz due to the shorter wavelength and dominance of inner resonance. Consequently, both resonances lead to dissipation of incident electromagnetic wave energy as a result of the high ohmic loss in HGAF pattern layer. In addition, the HGAF pattern layer provides a lower quality factor and facilitates the merging of the two absorptions, thereby achieving an absorption efficiency of 90 % at the center frequency.

The equivalent circuit model of GAF MMA cell is presented in Fig. 2(h). Fig. 2(f) shows that a strong current passed through the patterned layer circle. Moreover, Fig. S2 shows the electric field distribution of HGAF pattern layer at 5.36 GHz and 16.00 GHz, which suggests a strong electric field exists between the two neighboring units. Consequently, the HGAF pattern layer is characterized by a combination of resistance–inductance–capacitance. The polyimide medium layer, the air layer, and the LGAF layer are modeled as two transmission line segments and a short-circuit wire respectively.

The reflection coefficient (Γ) of the circular can be calculated by

$$\Gamma = \frac{Y_0 - Y_{in}}{Y_0 + Y_{in}} \tag{2}$$

where Y_0, Y_{in} is the admittance of the air and input admittance. When $\mathrm{Im}[Y_{in}] = 0$, $\mathrm{Re}[Y_{in}] = \mathrm{Re}[Y_A] \approx Y_0$ the reflection coefficient (Γ) is close to 0 and the absorber can achieve perfect absorption. To illustrate the accuracy of the proposed ECM with respect to the GAF MMA design parameters, we adjusted the values of the ECM components in ADS to produce compliant absorption bands. The parameters are optimized to achieve the desired performance as follows: $R = 190.64\ \Omega$, $L = 2.5119\ nH$, $C = 0.1184\ pF$, $Z_0 = 377\ \Omega$, $Z_1 = 148\ \Omega$, $Z_2 = 377\ \Omega$, $h_1 = 1.07$ mm, $h_2 = 4.70$ mm. As shown in Fig. S5, the reflection coefficient obtained from ECM and full-wave simulator CST achieved a good fit.

To clarify the absorption mechanism of the GAF MMA clearly, the calculated equivalent impedance by the parameter inversion method is shown in Fig. 2(i) and (j) Similarly, the matching degree between the absorber and the free space is quantified by means of the following formula

$$Z = \left|(Z_{real} - 1) + iZ_{imag}\right| \tag{3}$$

At the two resonant frequency points of 5.36 GHz and 16.00 GHz, the value of formula (3) approaches zero, indicating the high matching with impedance of free space and the low reflection of electromagnetic waves into free space. Only a minimal portion of electromagnetic waves is reflected to free space, resulting in an absorption efficiency of GAF MMA exceeding 90 % across the entire frequency spectrum.

3.2. Fabrication and experiment

To verify the performance of the designed GAF ultra-wideband MMA, a 20 × 20 cycle array is fabricated using graphene ink with a sheet resistance of 57 Ω/sq. The air layer in the middle is replaced by a foam dielectric substrate with a dielectric constant of 1.07. The LGAF layer comprises graphene-assembled films with a resistance of 0.03 Ω/sq. The actual prototype, screen-printing machine, and screen plate used in the experiment are shown in Fig. S6. During the printing process, the platform, substrate, and screen remain fixed while the graphene ink is printed to the polyimide substrate through the patterned mesh using a scraper. Subsequently, the polyimide substrate with printed ring pattern undergoes thermal treatment in an oven at 60 °C for half an hour, exhibiting remarkable flexibility as depicted in Fig. 3(a). Finally, the layers are securely assembled with double-sided tape to form GAF MMA, which possesses a weight of 44.06 g (Fig. 3(b)) and exhibits a surface density of 0.049 g/cm^2. As depicted in Fig. 3(c), the fabricated GAF MMA is measured in the anechoic chamber. The GAF MMA is placed 3 m away from the standard gain horn antenna to comply with the far-field measurement requirements. The measured results exhibit excellent agreement with the simulated results, as depicted in Fig. 4(d). Within the frequency range of 4.24–17.90 GHz, the GAF MMA demonstrates absorption efficiency exceeding 90 %, resulting in a relative bandwidth of 123.4 %. Specifically, absorption rates of 98.3 % at 4.75 GHz and 97.6 % at 16.43 GHz are achieved. The absorption of the fabricated GAF MMA at different incident angles is shown in Fig. 3(e) and (f), both simulated and measured. Within the incidence angle range of 0°–30°, the absorber ensures over 85 % absorption within the working frequency band (4.10–17.80 GHz), which proved that GAF MMA has good angular stability.

3.3. Experiment for extremes

The chemical stability of graphene, as a type of carbon material, is exceptionally remarkable. To evaluate the performance in extreme environments, the GAF MMA is treated in extreme scenarios of acidic, alkaline, salt spray, high-humidity, high-temperature, and low-temperature environments, and then measured. To provide evidence, the GAF MMA is subjected to a 0.5 mol/L sulfuric acid solution, a 0.1 mol/L sodium hydroxide solution, and a 5 % concentration sodium chloride solution for 72 h through spray deposition. Additionally, another set of samples is exposed to a relative humidity exceeding 80 % for the same duration. Two more groups of samples are subjected to temperatures of 120 °C and −196 °C for 3 h each. Subsequently, all six GAF MMA are rinsed with distilled water and air-dried before measuring their performances. The absorption rates corresponding to these six experimental groups are presented in Fig. 4.

Although there is a slight fluctuation observed in the absorption curve within the operating bandwidth of the GAF absorbers treated with sulfuric acid solution and the sodium chloride solution, they exhibit an absorption rate of more than 90 % in the frequency band of 4.90–17.70 GHz. The relative bandwidth of the GAF MMAs in these experimental

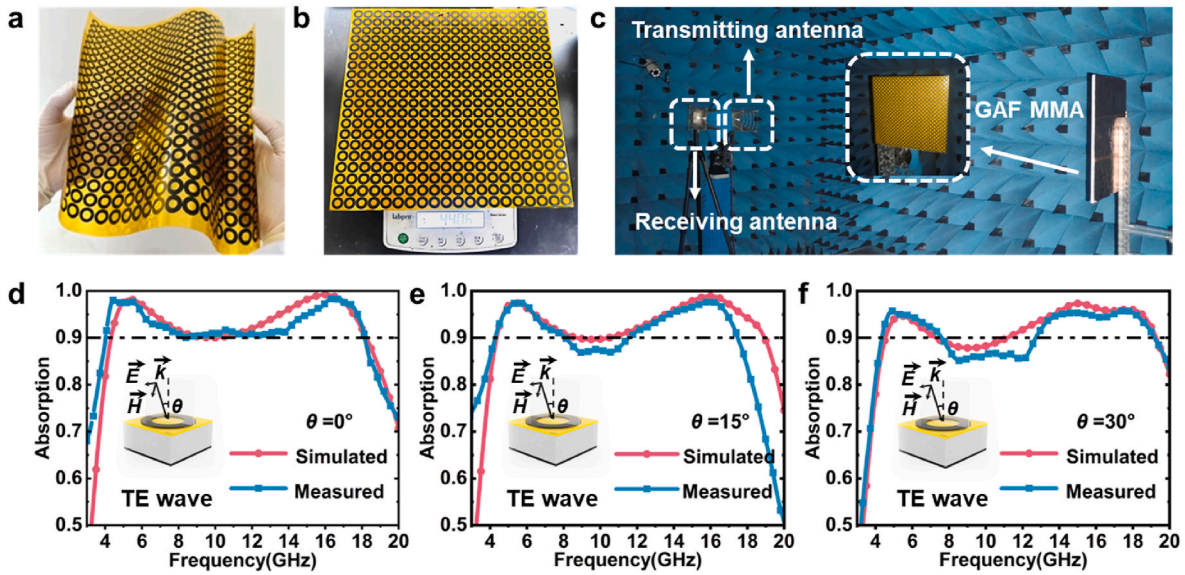

Fig. 3. (a) Flexible property of the HGAF pattern layer with polyimide substrate. (b) Digital photo of GAF MMA on an electronic balance. (c) Measurement environment of GAF MMA in an anechoic chamber. (d)–(f) Measured absorption and simulated absorption at incident angles of 0° (d), 15°(e), and 30°(f).

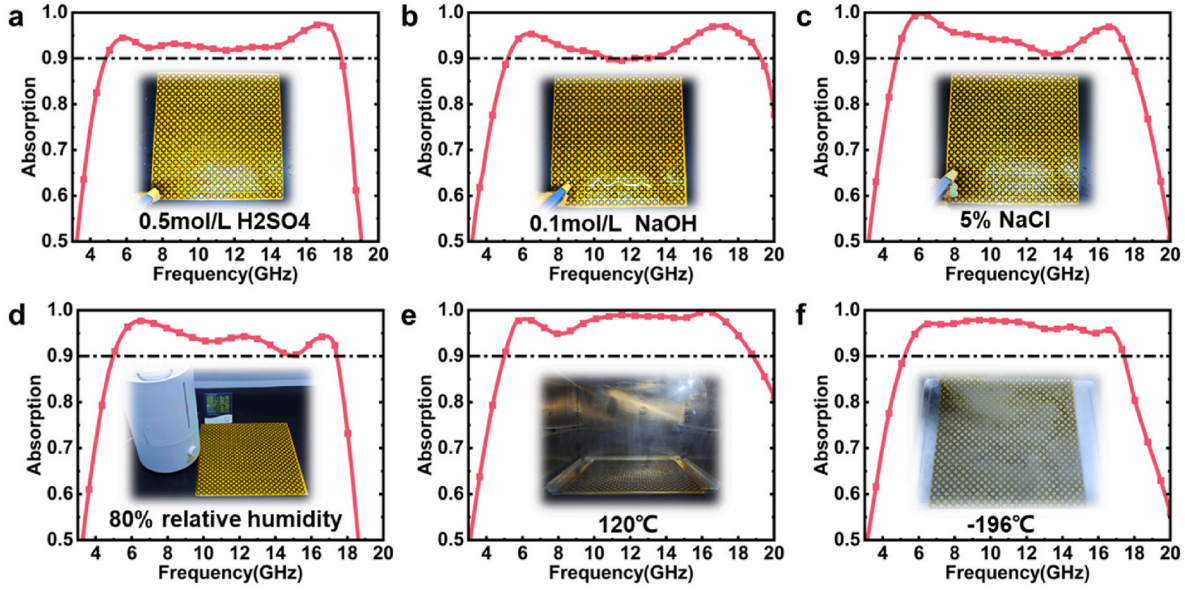

Fig. 4. The absorption of GAF MMA is measured under extreme acidic (a), alkaline (b), salt spray (c), high-humidity of 80 % (d), high-temperature of 120 °C (e), and low-temperature of −196 °C (f).

groups is 113.3 %. Similarly, after treatment with sodium hydroxide solution, the desired bandwidth of the absorber is 114.4 %, and more than 90 % of the absorption frequency range is 5.20–19.10 GHz. In this sample treated in a high-humidity environment, the GAF MMA operates at a bandwidth of 5.10–17.30 GHz, with a relative bandwidth of 108.90 %. Furthermore, under high-temperature treatment, the GAF MMA demonstrates an absorption efficiency exceeding 90 % across the frequency range of 5.10–18.70 GHz, exhibiting a relative bandwidth of 114.3 %. Moreover, after low-temperature treatment, the GAF MMA has more than 90 % effective absorption in 5.20–17.30 GHz with a relative bandwidth of 107.5 %. All experimental results demonstrate the effective electromagnetic wave absorption capability of the designed GAF MMA in various extreme environments, including acidic, alkaline, salt, high-humidity, high-temperature, and low-temperature environments. Although there are slight discrepancies between the working bandwidths observed in each group and those predicted by simulations, overall consistency with simulation outcomes remains remarkably high.

4. Conclusion

In conclusion, a highly reliable and ultra-wideband metamaterial absorber based on graphene-assembled films with varying resistances is presented. The GAF MMA consists of four-layer structures: a high-resistance graphene pattern layer, a polyimide medium layer, an air layer, and a low-resistance graphene reflection layer. Simulation and measurement results show that the absorption frequency band covers 4.24–17.90 GHz, and the relative bandwidth reaches 123.4 %. With the incident angle of the EM wave increasing from 0° to 30°, the designed GAF MMA also has the characteristics of large-angle stability. In addition, using graphene-assembled films allows the absorber to maintain high absorption (90 %) in acid, alkali, salt spray, high-humidity, high-temperature, and low-temperature environments. All results proved that

the designed ultra-wideband MMA can efficiently absorb electromagnetic waves and has great potential in applying electromagnetic protection under extreme conditions.

CRediT authorship contribution statement

Yu Zhou: Writing – original draft, Validation, Methodology, Investigation, Conceptualization. **Bilei Zhou:** Validation, Supervision, Investigation. **Shiyi Jin:** Validation, Investigation. **Zhi Luo:** Validation, Conceptualization. **Wei Qian:** Investigation. **Jiannan Guo:** Validation. **Baowen Li:** Supervision. **Haoran Zu:** Supervision. **Rongguo Song:** Supervision. **Daping He:** Supervision, Funding acquisition.

Declaration of competing interest

The authors declare that they have no known competing financial interests or personal relationships that could have appeared to influence the work reported in this paper.

Acknowledgments

This research was funded by the National Natural Science Foundation of China (51672204, 51701146, 62001338), China Postdoctoral Science Foundation Grant 2023M744293, and Foundation of the National Key Laboratory of Microwave Imaging Technology and Fundamental Research Funds for the Central Universities (WUT: 2024IVA031).

Appendix A. Supplementary data

Supplementary data to this article can be found online at https://doi.org/10.1016/j.carbon.2024.119534.

References

[1] P. Ranjan, A. Choubey, S.K. Mahto, et al., A novel ultrathin wideband metamaterial absorber for X-band applications, J. Electromagn. Waves Appl. 33 (17) (2019) 2341–2353.
[2] C. Barde, A. Choubey, R. Sinha, et al., A compact wideband metamaterial absorber for Ku band applications, J. Mater. Sci. Mater. Electron. 31 (19) (2020) 16898–16906.
[3] S. Hannan, M.T. Islam, M.R.I. Faruque, et al., Polarization-independent perfect metamaterial absorber for C, X, and, Ku band applications, J. Mater. Res. Technol. 15 (2021) 3722–3732.
[4] N.I. Landy, S. Sajuyigbe, J.J. Mock, et al., Perfect metamaterial absorber, Phys. Rev. Lett. 100 (20) (2008) 207402.
[5] W. Luo, S. Yan, J. Zhou, Ceramic-based dielectric metamaterials, Interdisciplinary Materials 1 (1) (2022) 11–27.
[6] J. Chen, S. Hu, S. Zhu, et al., Metamaterials: from fundamental physics to intelligent design, Interdisciplinary Materials 2 (1) (2023) 5–29.
[7] C. Barde, A. Choubey, R. Sinha, Wide band metamaterial absorber for Ku and K band applications, J. Appl. Phys. 126 (17) (2019).
[8] B. Mulla, C. Sabah, Perfect metamaterial absorber design for solar cell applications, Waves Random Complex Media 25 (3) (2015) 382–392.
[9] Y.I. Bdulkarim, O. Altintas, A.S. Karim, et al., Highly sensitive dual-band terahertz metamaterial absorber for biomedical applications: simulation and experiment, ACS Omega 7 (42) (2022) 38094–38104.
[10] M. Amiri, F. Tofigh, N. Shariati, et al., Review on metamaterial perfect absorbers and their applications to IoT, IEEE Internet Things J. 8 (6) (2020) 4105–4131.
[11] S.A.M. Ali, M. Abu, S.N. Zabri, A review: the development of metamaterial absorber, Int. J.Integrated Eng. 12 (1) (2020) 72–80.
[12] B.X. Wang, C. Xu, G. Duan, et al., Review of broadband metamaterial absorbers: from principles, design strategies, and tunable properties to functional applications, Adv. Funct. Mater. 33 (14) (2023) 2213818.
[13] B. Wang, B.Y. Gong, M. Wang, et al., Dendritic wideband metamaterial absorber based on resistance film, Appl. Phys. A 118 (2015) 1559–1563.
[14] H. Sheokand, S. Ghosh, G. Singh, et al., Transparent broadband metamaterial absorber based on resistive films, J. Appl. Phys. 122 (10) (2017).
[15] X. Ling, Z. Xiao, X. Zheng, et al., Ultra-broadband metamaterial absorber based on the structure of resistive films, J. Electromagn. Waves Appl. 30 (17) (2016) 2325–2333.
[16] S. Ghosh, S. Bhattacharyya, Y. Kaiprath, et al., Bandwidth-enhanced polarization-insensitive microwave metamaterial absorber and its equivalent circuit model, J. Appl. Phys. 115 (10) (2014).
[17] P.V. Tuong, J.W. Park, Y.J. Kim, et al., Broadband reflection of polarization conversion by 90 in metamaterial, J. Kor. Phys. Soc. 64 (2014) 1116–1119.
[18] H. Li, L.H. Yuan, B. Zhou, et al., Ultrathin multiband gigahertz metamaterial absorbers, J. Appl. Phys. 110 (1) (2011).
[19] R.M.H. Bilal, M.A. Baqir, P.K. Choudhury, et al., Wideband microwave absorber comprising metallic split-ring resonators surrounded with E-shaped fractal metamaterial, IEEE Access 9 (2021) 5670–5677.
[20] C. Long, S. Yin, W. Wang, et al., Broadening the absorption bandwidth of metamaterial absorbers by transverse magnetic harmonics of 210 mode, Sci. Rep. 6 (1) (2016) 21431.
[21] F. Ding, Y. Cui, X. Ge, et al., Ultra-broadband microwave metamaterial absorber, Appl. Phys. Lett. 100 (10) (2012).
[22] Z. Du, J. Liang, T. Cai, et al., Ultra-light planar meta-absorber with wideband and full-polarization properties, Opt Express 29 (5) (2021) 6434–6444.
[23] J. Yu, W. Jiang, S. Gong, Wideband angular stable absorber based on spoof surface plasmon polariton for RCS reduction, IEEE Antenn. Wireless Propag. Lett. 19 (7) (2020) 1058–1062.
[24] Cheng Y. Zhi, Y. Wang, Y. Nie, et al., Design, fabrication, and measurement of a broadband polarization-insensitive metamaterial absorber based on lumped elements, J. Appl. Phys. 111 (4) (2012).
[25] S.J. Li, P.X. Wu, H.X. Xu, et al., Ultra-wideband and polarization-insensitive perfect absorber using multilayer metamaterials, lumped resistors, and strong coupling effects, Nanoscale Res. Lett. 13 (2018) 1–13.
[26] S. Fan, Y. Song, Ultra-wideband flexible absorber in microwave frequency band, Materials 13 (21) (2020) 4883.
[27] D. Lim, S. Lim, Ultrawideband electromagnetic absorber using sandwiched broadband metasurfaces, IEEE Antenn. Wireless Propag. Lett. 18 (9) (2019) 1887–1891.
[28] K. Ling, M. Yoo, S. Lim, Frequency tunable metamaterial absorber using hygroscopicity of nature cork, IEEE Antenn. Wireless Propag. Lett. 14 (2015) 1598–1601.
[29] Y. Zhang, P. Zhao, Q. Lu, et al., Functional additive manufacturing of large-size metastructure with efficient electromagnetic absorption and mechanical adaptation, Compos. Appl. Sci. Manuf. 173 (2023) 107652.
[30] Y. Zhang, H. Dong, C. Yu, et al., Metastructure based broadband structural stealth with material-structure-function integration, Compos. Sci. Technol. 253 (2024) 110661.
[31] K. Zhang, Y. Liu, Y. Liu, et al., Tracking regulatory mechanism of trace Fe on graphene electromagnetic wave absorption, Nano-Micro Lett. 16 (1) (2024) 66.
[32] R. Song, Z. Wang, H. Zu, et al., Wideband and low sidelobe graphene antenna array for 5G applications, Sci. Bull. 66 (2) (2021) 103–106.
[33] W. Yang, C. Wang, Graphene and the related conductive inks for flexible electronics, J. Mater. Chem. C 4 (30) (2016) 7193–7207.
[34] R. Song, Q. Wang, B. Mao, et al., Flexible graphite films with high conductivity for radio-frequency antennas, Carbon 130 (2018) 164–169.
[35] R. Song, B. Mao, Z. Wang, et al., Comparison of copper and graphene-assembled films in 5G wireless communication and THz electromagnetic-interference shielding, Proc. Natl. Acad. Sci. USA 120 (9) (2023) e2209807120.
[36] S.D. Assimonis, V. Fusco, Polarization insensitive, wide-angle, ultra-wideband, flexible, resistively loaded, electromagnetic metamaterial absorber using conventional inkjet-printing technology, Sci. Rep. 9 (1) (2019) 12334.
[37] S. Kalraiya, R.K. Chaudhary, M.A. Abdalla, Design and analysis of polarization independent conformal wideband metamaterial absorber using resistor loaded sector shaped resonators, J. Appl. Phys. 125 (13) (2019).
[38] C. Zhang, J. Yang, W. Cao, et al., Transparently curved metamaterial with broadband millimeter wave absorption, Photon. Res. 7 (4) (2019) 478–485.
[39] X. Luo, B. Cao, J. Zhang, et al., High-performance water-based metamaterial wave absorber based on ku band, Plasmonics (2024) 1–9.
[40] M. Yoo, S. Lim, Polarization-independent and ultrawideband metamaterial absorber using a hexagonal artificial impedance surface and a resistor-capacitor layer, IEEE Trans. Antenn. Propag. 62 (5) (2014) 2652–2658.
[41] M.D. Banadaki, A.A. Heidari, M. Nakhkash, A metamaterial absorber with a new compact unit cell, IEEE Antenn. Wireless Propag. Lett. 17 (2) (2017) 205–208.
[42] X. Huang, H. Yang, D. Wang, et al., Calculations of a wideband metamaterial absorber using equivalent medium theory, J. Phys. Appl. Phys. 49 (32) (2016) 325101.